Alkali Ion-Controlled Excited-State Ordering of Acetophenones Included in Zeolites: Emission, Solid-State NMR, and Computational Studies[†]

J. Shailaja,[‡] P. H. Lakshminarasimhan,[‡] Ajit R. Pradhan,[‡] R. B. Sunoj,[§] Steffen Jockusch,[||] S. Karthikeyan,[‡] Sundararajan Uppili,[‡] J. Chandrasekhar,[§] Nicholas J. Turro,[||] and V. Ramamurthy*,[‡]

Department of Chemistry, Tulane University, New Orleans, Louisiana 70118, Department of Organic Chemistry, Indian Institute of Science, Bangalore 560012, India, and Department of Chemistry, Columbia University, New York, New York 10027

Received: July 17, 2002; In Final Form: October 13, 2002

The nature of the lowest triplet excited state of acetophenones included in zeolites has been inferred through steady-state and time-resolved emission spectra. Acetophenone shows cation-dependent state switching. Within NaLiY and NaY zeolites, the emitting state is identified to have $\pi\pi^*$ character, whereas in NaRbY and NaCsY, two emissions characteristic of $n\pi^*$ and $\pi\pi^*$ were observed. In contrast, 4′-methoxyacetophenone does not show cation-dependent state switching; in all alkali cation-exchanged zeolites, the lowest triplet is identified to have $\pi\pi^*$ character. The results are attributed to a specific cation−acetophenone interaction. Static, MAS, and CP-MAS spectra of ^{13}C-enriched acetophenone included in MY zeolites confirm the presence of such an interaction. The data reveals that the extent of interaction, as reflected by the molecular mobility, depends on the cation. Small cations such as Li^+ and Na^+ interact strongly whereas large cations such as Rb^+ and Cs^+ interact weakly with acetophenone. Consistent with these trends, small cations are found to switch the lowest triplet to $\pi\pi^*$ character, whereas the large cations leave the $n\pi^*$ and $\pi\pi^*$ triplet states of acetophenone close to each other. Computational studies provide strong support for these interpretations. B3LYP/6-31G* calculations were carried out on acetophenone and 4′-methoxyacetophenone as well as their Li^+ and Na^+ complexes. Geometries with cations bound to the carbonyl, phenyl, and methoxy groups were examined. The most-stable structures involve a cation−carbonyl interaction, which stabilizes the n orbital and, in turn, destabilizes the $n\pi^*$ triplet state. Excited-state energetics were quantified using TDDFT/6-31+G* calculations. Consistent with experimental observations, acetophenone and 4′-methoxyacetophenone are predicted to have $n\pi^*$ and $\pi\pi^*$ as their lowest triplet states, respectively. Complexation with Li^+ or Na^+ is predicted to lead to a $\pi\pi^*$ triplet as the lowest excited state for both compounds. The present study, combining steady-state and time-resolved emission spectra, solid state NMR, and computations, demonstrates the occurrence of cation-dependent state switching in acetophenones and offers an internally consistent explanation of the effect in terms of specific cation−carbonyl interaction.

The generality and simplicity of the orbital-based nomenclature for electronic transitions introduced by Kasha[1] allowed photochemists to classify and predict photoreactions on the basis of the orbital nature of the excited state.[2] Since the pioneering studies by Hammond on the photoreduction of benzophenone, it has become clear that in carbonyl compounds the $n\pi^*$ state is more reactive than the $\pi\pi^*$ state.[3] This has led photochemists to seek conditions under which a given carbonyl compound would possess $n\pi^*$ as the lowest excited state. Since the early 1960s, it has been known that aryl−alkyl ketones and diaryl ketones may possess closely placed $n\pi^*$ and $\pi\pi^*$ triplet states.[4] The relative energies of the two states, each with its own distinctive photophysical and photochemical behavior, have been manipulated by chemical substitution and the polarity of the medium.[5] Some ketones such as acetophenone (ACP) have their

two triplets so close in energy that they may be inverted simply by adjusting the polarity of the solvent. For example, in hydrocarbon glass, the emission from acetophenone is characteristic of the $n\pi^*$ triplet, whereas in polar hydrogen-bonding media such as silica gel, a long-lived (∼300 ms) emission characteristic of the $\pi\pi^*$ triplet is observed.[6] However, phosphorescence emission from 4′-methoxyacetophenone (MACP) is independent of the medium, and the nature of the lowest triplet remains $\pi\pi^*$ in character both in polar and nonpolar media.

By employing the structural resolution of the emission spectrum and the lifetime of the emitting state, we have identified the nature of the lowest triplet of ACP within MY (M = Li^+, Na^+, K^+, Rb^+ and Cs^+; Si/Al 2.4) zeolites to be dependent on the alkali ion. Results of a comprehensive investigation involving photophysical, solid-state NMR, and computational studies, which have allowed us to establish that cations interact with ACP included in MY zeolites, the lowest triplet of ACP has $\pi\pi^*$ character within NaLiY, NaY, and NaKY, and both $\pi\pi^*$ and $n\pi^*$ are close by within NaRbY and NaCsY, are presented in this report. The alkali ion-prompted triplet-state switching is very valuable to bring the $\pi\pi^*$ state
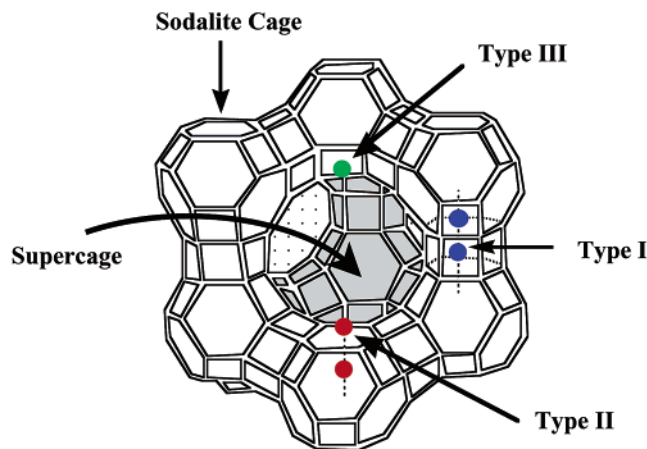
Figure 1. Structure of the zeolite supercage. Positions of cations are identified as Types I, II, and III.

below the $n\pi^*$ triplet and thus open up new reaction pathways that otherwise would remain latent. The alkali ions are more powerful than even polar solvents in inducing state switching. We have recently exploited this strategy to alter the chemical behavior of excited enones and dienones.[7] The phenomenon of state switching we describe here may not be restricted to zeolites, and one might even be able to induce state switching with alkali metal ions provided they are free to interact with the solute molecules.[8] This aspect needs further exploration.

An important assumption in the interpretation of our photophysical results is that aryl alkyl ketones adsorb within MY zeolites through interaction with cations present in the supercages. To appreciate the presentation, it is essential to have a brief background of the internal structure of zeolite Y and cation–organic interactions within zeolites. The internal structure of the faujasite class of zeolites is characterized by a 3D network of supercages (large voids ca. 13 Å in diameter within which adsorbed guest molecules are located) interconnected by tetrahedrally disposed windows (ca. 8 Å diameter, Figure 1).[9] Charge-compensating cations are located at three different sites within the zeolite framework, of which only two (Types II and III) are expected to be readily accessible to the adsorbed organic molecule.[10] The Y zeolite used in this study has only Types I and II sites occupied. A variety of techniques have demonstrated that cation–guest interaction plays an important role during the adsorption of organic molecules within MY zeolites.[11] Cation–π interaction (also known as cation–quadrupolar interaction)[12] has been recognized as the main force of binding between aromatic guest molecules and the zeolite supercage. However, when a benzene ring contains a polar group such as nitro (dinitrobenzene), the primary interaction is between the cation and the oxygens of the nitro group (not the π cloud of the phenyl ring).[13] Such a type of dipolar interaction between the cation and the guest predominates even in nonaromatic molecules such as hydrofluorocarbons within NaY.[14] A point we wish to emphasize is that the cations are likely to move from their original location when the cation–guest interaction is stronger than the cation–zeolite surface interaction. Examples include nitrobenzene, hydrofluorocarbons, and water.[13,14,15] On the basis of literature precedence on related systems,[11–15] we believe that aryl–alkyl ketones would be stabilized within the MY zeolite via either a cation–π or a cation–carbonyl dipolar interaction. We have employed [13]C Bloch decay with high-power ^{1}H decoupling acquired under static and magic-angle spinning (MAS) and [1]H–[13]C cross polarization under magic-angle spinning (CP-MAS) NMR spectral measurements to probe the existence of an interaction between the zeolite and ACP. Although these

measurements confirm the presence of an interaction between the alkali ion and ACP, they do not provide information concerning the structure of the cation–ACP complex. In this context, ab initio computations of "alkali ion⋯ACP" and "alkali ion⋯MACP" complexes have been very valuable.

Our computational studies are designed to address the following questions: (a) Can we reproduce the triple-state ordering and energies of unperturbed ACP and MACP? (b) What will be the preferred binding modes and corresponding binding affinities of alkali metal ions with these two ketones? (c) What are the triplet-state ordering and energies of the alkali ion-bound ketones? To our knowledge, there are no computational studies addressing the above questions related to aryl alkyl ketones. However, recently, computations directed toward understanding the excited-state properties of aliphatic ketones and aldehydes have been performed, and in this context among various methods, time-dependent density functional theory (TDDFT) has been reported to yield results consistent with experiments.[16] We have used B3LYP/6-31G* calculations to compute the geometries of unperturbed and alkali ion-bound ACP and MACP and the excitation energies (adiabatic and vertical) of the lowest triplet. Single-point calculations were carried out using CIS and TDDFT procedures to obtain the triplet-state ordering and energies of T_1 and T_2 for the unperturbed and alkali ion-bound ACP and MACP.

Results

Photophysical Studies. For photophysical studies, ACP and MACP were introduced into the zeolite by stirring 1 mg of the ketone with 300 mg of the MY zeolite in 5 mL of hexane for 3 h. One should note that when Li$^+$, K$^+$, Rb$^+$, and Cs$^+$ were exchanged for Na$^+$ the exchange level was less than 100%. On the basis of ICP analysis, the exchange levels of Li$^+$, K$^+$, Rb$^+$, and Cs$^+$ were assessed to be 64, 84, 68, and 62%, respectively. Therefore, they should ideally be represented as NaMY where M = Li$^+$, K$^+$, Rb$^+$, and Cs$^+$. Type I cations mostly remain unexchanged. Removal of hexane by filtration and drying the resulting zeolite powder under reduced pressure ($\sim$10^{-3} Torr) gave the sample containing the ketone in the zeolite. Generally, the loading level was kept at $\sim$1 molecule per 10 supercages. UV diffuse-reflectance spectra confirmed the presence of ketones. Samples were taken in quartz ESR tubes, and the emission was recorded in a front face mode. The phosphorescence emission spectra (77 K) of MACP included in NaY and NaCsY were similar and structureless, suggesting that the emitting state has the same character ($\pi\pi^*$) in both media. However, ACP and substituted acetophenones, which are known to have $n\pi^*$ as the lowest triplet in nonpolar media and the $\pi\pi^*$ state in very polar media, showed emissions with differing characteristics within NaY and NaCsY. Phosphorescence spectra recorded at 77 K from ACP and 4$'$-fluoroacetophenone included in NaY and NaCsY are shown in Figure 2. As seen in Figure 2, the emission is broad in NaY and slightly structured in NaCsY. Generally, the spectra of ACP included in either methylcyclohexane or methanol–ethanol glass show more structure than that of ACP included in NaCsY. 4$'$-Trifluoromethylacetophenone, 3$'$-cyanoacetophenone, 3$'$-fluoroacetophenone, 3$'$-chloroacetophenone, and 2$'$-fluoroacetophenone showed emissions having characteristics similar to that of acetophenone. An obvious interpretation of these results is that these ketones have a $\pi\pi^*$ triplet within NaY and close-lying $n\pi^*$ and $\pi\pi^*$ triplets (two emitting states) within NaCsY. On the basis of an earlier report on silica gel,[5] it is tempting to attribute the observed effect to the surface silanol groups of
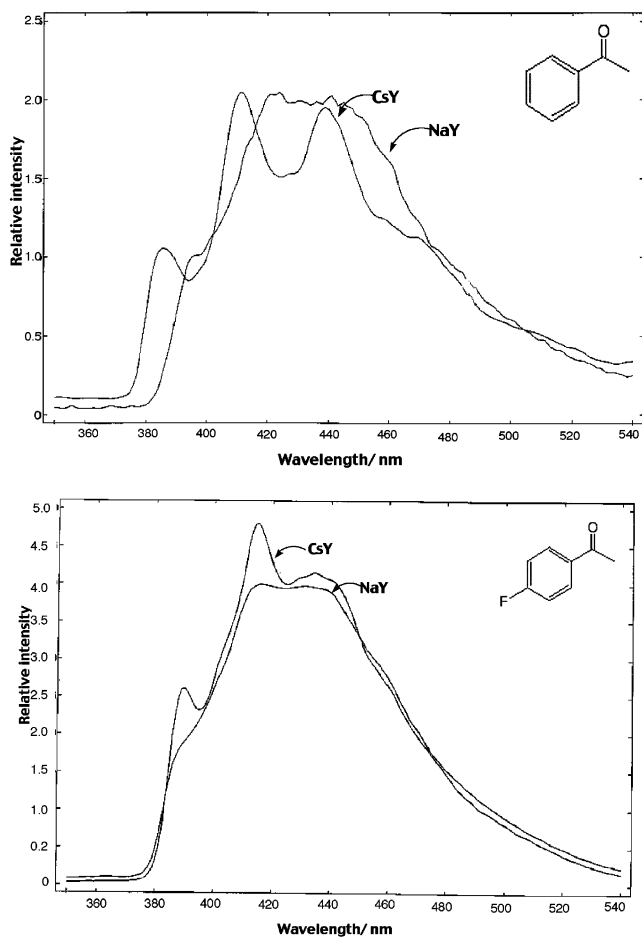
Figure 2. Phosphorescence emission spectra of acetophenone and 4′-fluoroacetophenone recorded at 77 K in NaY and NaCsY zeolites.

Figure 3. Time-resolved phosphorescence spectra of ACP@NaY, ACP@NaCsY, and MACP@NaCsY recorded 1−2 ms and 25−40 ms after the lamp pulse ($\lambda_{ex} = 320$ nm) at 77 K.

zeolite Y. However, it should be noted that the supercages of MY zeolites (Si/Al 2.4) contain very few silanol groups.[9]

It has been reported that the spectral features alone are not sufficient to identify the nature of the emitting state.[17] To assign the nature of the emitting state of ACP within MY zeolites unequivocally, we have recorded the time-resolved emission spectra and measured the triplet lifetimes of ACP and MACP included in MY zeolites. The emission spectra of ACP included in dry NaY (1 molecule per 10 supercages) at different time intervals are shown in Figure 3. Clearly independent of the time interval, the emission is structureless, a characteristic of a $\pi\pi^*$ state. Consistent with this assignment, the lifetime of the emission was measured to be 420 ms. The observed time-resolved emission of ACP included in NaCsY showed slightly different features at early and late time intervals (Figure 3). At early times (1−2 ms), the phosphorescence spectrum is structured, whereas at later times (25−40 ms), it is broad and less structured. As would be expected, the decay kinetics of the phosphorescence of ACP included in NaCsY (Figure 4) consist of two components with lifetimes of ∼1.5 and ∼170 ms. Because of the short phosphorescence lifetime and structured spectrum, it was concluded that the short-lived component is due to an $n\pi^*$ triplet. The long-lived component is consistent with phosphorescence from a $\pi\pi^*$ triplet state. Phosphorescence lifetime measurements were also performed for ACP included within NaLiY, NaKY, and NaRbY (Figure 4). Similar to ACP within NaY, phosphorescence from a $\pi\pi^*$ triplet state alone was observed within NaLiY and NaKY. Two-component phosphorescence, attributable to $n\pi^*$ and $\pi\pi^*$ triplets, was observed within NaRbY (Figure 4). It is noteworthy that the
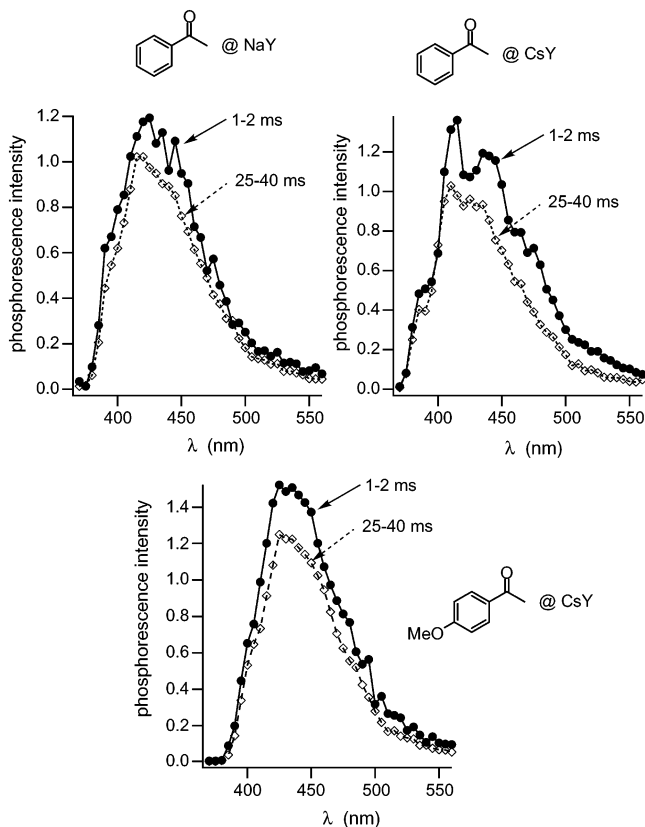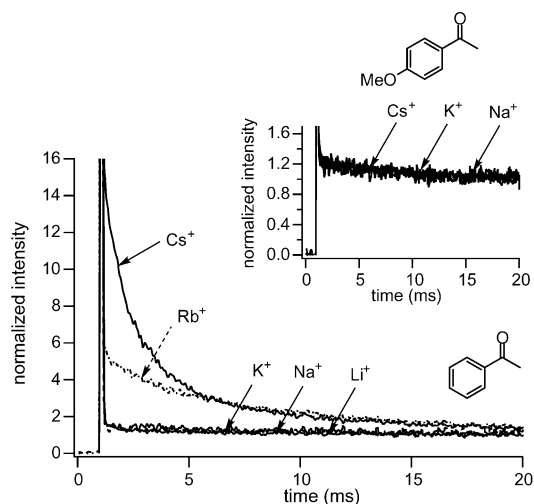

Figure 4. Normalized phosphorescence decay kinetics of ACP and MACP (inset) in the cation-exchanged Y zeolite ($\lambda_{ex} = 320$ nm, $\lambda_{em} = 430$ nm) at 77 K.

phosphorescence lifetime of ACP derived from the $\pi\pi^*$ triplet state (long-lived component) decreases with increasing atomic number of the alkali ion (420, 250, 220, and 170 ms; Na^+, K^+, Rb^+, and Cs^+, respectively). The observed trend is consistent with the expected heavy-atom (cation) effect when the intersystem crossing is from a $\pi\pi^*$ triplet to a singlet ground state.[18] Although the lifetime was slightly dependent on the loading level (varied between 400 ms for 2 molecule per 1 supercage to 550 ms for 1 molecule per 25 supercages), the structure of the emission remained broad within NaY independent of the loading level of ACP (varied between 1 molecule per 25 supercages to 2 molecules per 1 supercage).
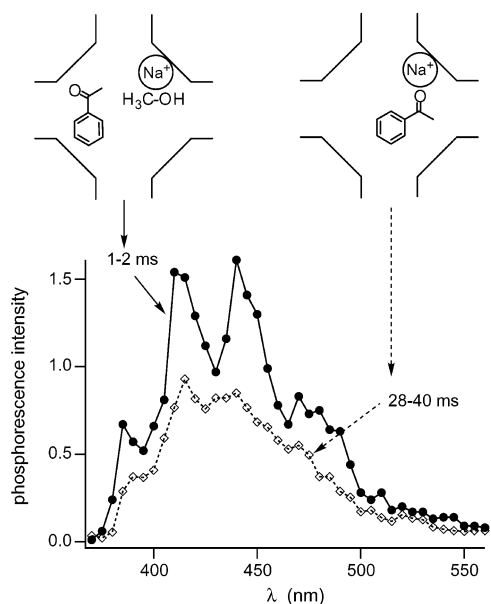
Figure 5. Time-resolved phosphorescence spectra of methanol-treated ACP@NaY recorded 1−2 ms and 28−40 ms after the lamp pulse (λ_{ex} = 320 nm) at 77 K.

From the results presented above, it is clear that the nature of the emitting triplet in ACP switches from the $n\pi^*$ (nonpolar media) to $\pi\pi^*$ state within zeolites. Generally, such a switch is attributed to the polarity of the medium.[5,19] An indication that cation−carbonyl interaction, not polarity, is responsible for the state switch comes from the following experiment. When methanol vapor, a polar molecule, was introduced into ACP included NaY and equilibrated for 12 h, the emission became structured, and the lifetime, short (Figure 5, compare with Figure 3). At a short observation time scale (1−2 ms), a structured ($n\pi^*$ triplet state) phosphorescence emission was observed, and at longer time scales (28−40 ms), an unstructured ($\pi\pi^*$) phosphorescence emission was observed. With increasing amounts of methanol, the short-lived component ($n\pi^*$ triplet) increased, and the lifetime stabilized at ∼5 ms when the loading level of methanol reached 2 molecules per supercage. If polarity was responsible for the triplet-state switch within zeolites, one would have expected the polar methanol to stabilize the $\pi\pi^*$ state. The fact that upon introduction of methanol the emitting state became $n\pi^*$ (instead of remaining as $\pi\pi^*$ state) suggests that methanol must be intercepting the species (alkali ion) that is causing the state switch. It is likely that methanol oxygen, being a better Lewis base, competes favorably with the carbonyl oxygen for binding to the alkali ion. We propose that when methanol is introduced into the zeolite, ACP becomes free from the alkali ion and the lowest triplet regains its original $n\pi^*$ character (Figure 5).

Time-resolved phosphorescence emission measurements were also carried out with MACP loaded into alkali cation-exchanged Y zeolites. Phosphorescence spectra within NaY, NaKY, and NaCsY were structureless and decayed with lifetimes between 570 and 300 ms (Figure 4). Even in NaCsY, where ACP showed $n\pi^*$ emission, MACP showed emission only from $\pi\pi^*$ state. This suggests that the emitting triplet of MACP independent of the alkali ion remains $\pi\pi^*$ in character. The phosphorescence lifetimes decreased in the order NaY > NaKY > NaCsY (565, 510, 300 ms, respectively), and this is consistent with the observation made with ACP (heavy-atom effect).

Solid-State NMR Investigations. To gain information on the mobility (and indirectly on the forces that control the mobility) of acetophenone molecules within zeolites, we have
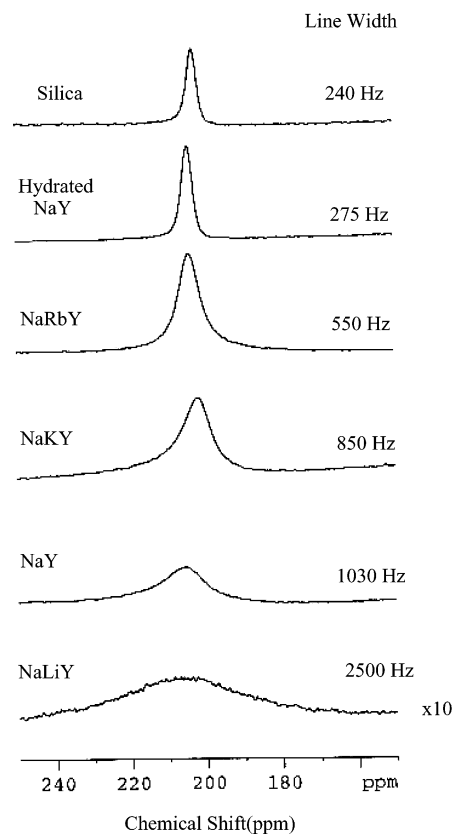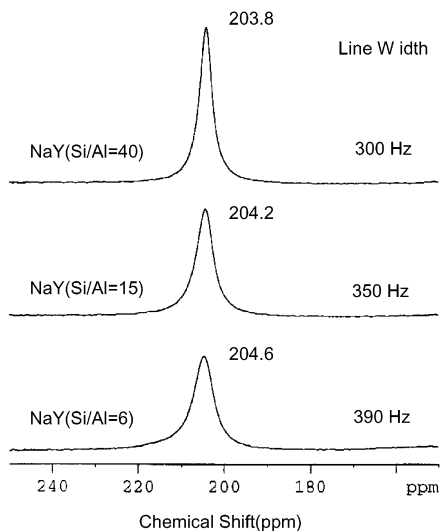

Figure 6. Static NMR spectra of ^{13}C-ACP included in NaLiY, NaY, NaKY, NaRbY, hydrated NaY, and silica gel.

recorded static, MAS, and CP-MAS NMR spectra of ^{13}C-enriched (carbonyl carbon) ACP included in NaLiY, NaY, NaKY, and NaRbY zeolites.[20] For comparison, spectra of ACP included in high-silica NaY (Si/Al 6, 15, and 40) and adsorbed on silica gel were also recorded. All experiments were done with zeolite samples having a loading level of 1 molecule of ACP per 4 supercages of MY (4 mg in ∼300 mg of zeolite). To avoid any loss of ACP during sample preparation, acetophenone was adsorbed within zeolites by simply mixing the acetophenone and zeolite as follows. In this procedure, known amounts of ACP and zeolite were ground together, transferred to a drying tube, sealed inside a drybox, and equilibrated at 60 °C under reduced pressure (1 × 10^{-3} Torr) for 12 h on a vacuum line. Static and MAS ^{13}C NMR spectra of the sample at various time intervals established that 12 h of heating (60 °C) at low pressure is long enough to distribute ACP uniformly over the zeolite samples. In addition to the line-width change, the ^{13}C chemical shift due to the carbonyl carbon gradually shifted from δ 202.3 (time zero) to δ 205 (time 12 h).

In Figures 6 and 7, static and MAS ^{13}C NMR spectra of ACP included within NaLiY, NaY, NaKY, and NaRbY and adsorbed on the silica surface are presented. The spectral line widths (fwhm) in static and MAS spectra provide information about the mobility of ACP; the larger the line width, the less the mobility. In general, under static conditions of spectral recording, rapid motions of the adsorbed molecules within a zeolite would remove the chemical shift anisotropy, leading to a sharper line. Under MAS conditions, in addition to removing broadening due to chemical shift anisotropy, any influence of dipolar interactions between spins is also removed.[20] Figures 6 and 7 clearly show that the lines are broad (both static and MAS spectra) in NaLiY and sharp on silica gel. A comparison of these two spectra alone suggests that either the Li cation or the confined space (silica pores are much larger than those of supercages, >100 Å vs

Alkali Ion-Controlled Ordering of Acetophenones

J. Phys. Chem. A, Vol. 107, No. 18, 2003 **3191**
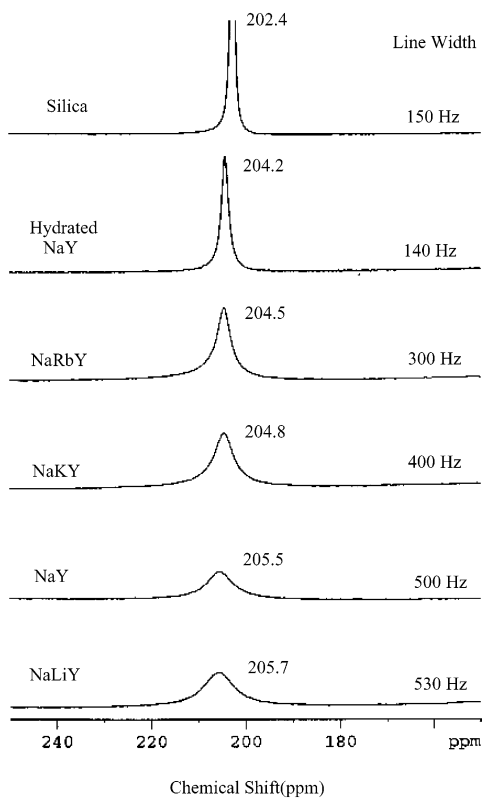
Figure 7. MAS NMR spectra of ^{13}C-ACP included in NaLiY, NaY, NaKY, NaRbY, hydrated NaY, and silica gel.

Figure 8. MAS NMR spectra of ^{13}C-ACP included in NaY for different Si/Al ratios.

<10 Å) must be responsible for the restricted mobility of ACP within NaLiY. However, when all MY and silica spectra presented in Figures 6 and 7 are compared, it is clear that the cations must play a role in the restriction of mobility of ACP molecules within MY zeolites. The line widths follow the trend Li$^+$ > Na$^+$ > K$^+$ > Rb$^+$; the higher the charge density, the larger the line width. In Figure 8, the MAS NMR spectra of ACP included in NaY with various Si-to-Al ratios are compared. High-silica Y (Si/Al 6, 15, and 40) zeolites have similar internal structures as Y zeolite (Si/Al 2.4) except that they contain smaller numbers of Na$^+$ ions.[9c] These samples are useful in differentiating between the importance of space and cation binding in the restriction of molecular mobility within Y zeolites. As seen in Figure 8, the signals are broader in samples with
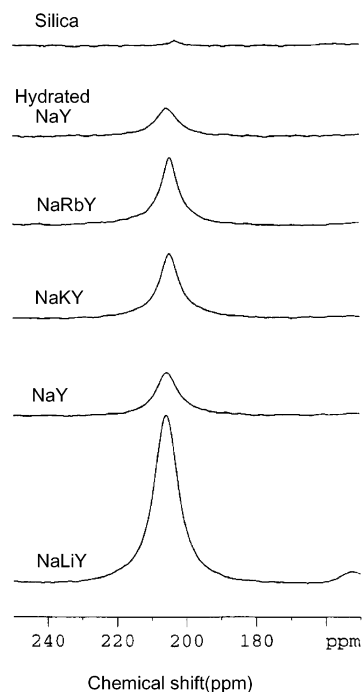
Figure 9. ^{1}H$-^{13}$C CP-MAS spectra of ^{13}C-ACP included in NaLiY, NaY, NaKY, NaRbY, hydrated NaY, and silica gel.

high aluminum (NaY, Si/Al 2.4) and sharper in samples with low aluminum (i.e., the less aluminum, corresponding to a smaller number of sodium ions). The above results suggest that cations play a role in controlling the mobility of ACP molecules within zeolites. Results obtained with water-saturated NaY samples are also consistent with the above conclusion. Moisture-exposed ACP included in a NaY sample gave sharp lines in static and MAS spectra (Figures 6 and 7), indicating that ACP molecules are no longer bound to the zeolite surface. It is quite likely that upon complexation of water molecules to Na$^+$, the ACP molecules become free and mobile. This observation is similar to the one made during photophysical studies where methanol (instead of water) was used as the competing molecule for complexation with sodium ions (Figure 5). An additional point is that the chemical shift of the carbonyl carbon is dependent on the medium. For example, the ^{13}C shift of the carbonyl in CDCl$_3$ solution is at δ 198.2, on silica, at δ 202.4, and within NaLiY, at δ 205.7. A significant change in the chemical shift between the solution and NaLiY suggests the existence of an interaction between the alkali ion and the carbonyl group. However, protonation or chemical bond formation between C=O and M$^+$ resulting in the development of a positive charge at the carbonyl carbon would have resulted in a larger shift ($\Delta\delta$ > 50).[21] Both the line width and observed small changes in the chemical shift suggest that there is an interaction between alkali ions and ACP within Y zeolites.

Further evidence in support of the presence of an ion$-$ACP interaction within zeolites come from ^{1}H$-^{13}$C CP-MAS spectra (Figure 9). In CP-MAS spectra, the intensity of the ^{13}C signal is inversely related to the mobility of the molecule. The efficiency of cross polarization depends on geometric factors and on the strength of ^{1}H$-^{13}$C dipolar coupling.[22] For samples with randomly oriented molecules where many orientations and distances are possible, the rate of cross polarization is maximized when molecules are relatively static. As seen in Figure 9, an intense signal in NaLiY and a very weak signal on silica are obtained, suggesting that the molecule is less mobile in NaLiY, a conclusion also reached on the basis of static and MAS spectra.
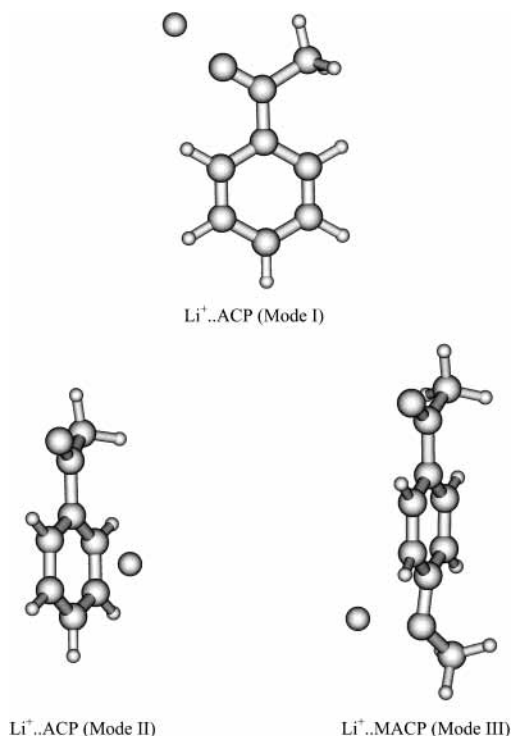
Figure 10. B3LYP/6-31G*-optimized geometries for the S_0 states of Li^+..ACP and Li^+..MACP systems.

The trend in signal intensity observed with various alkali ion-exchanged Y zeolites (NaLiY > NaY > NaKY > NaRbY) is the one expected if the ion−molecule interaction is controlling the mobility of ACP molecules within MY zeolites. In principle, the free volume of a supercage, rather than ion binding, may determine the mobility of ACP. Since the free volume within a supercage is expected to decrease with an increase in ion size,[23] the line width and intensity of signals should have followed the trend NaLiY < NaY < NaKY < NaRbY, opposite to that observed. Therefore, ion-binding is indicated to be the key factor controlling the mobility.

Computational Results. Both photophysical and solid-state NMR studies suggest that there is an interaction between the alkali ions and ACP included in zeolites. But neither of them provides any details about the structure and binding affinities of such interactions. We have resorted to a computational approach to gain more insight into the structure, energy, and electronic consequences of alkali metal ion−carbonyl interactions. We recognize that within a zeolite, as a result of the cations being bound to zeolite walls made up of a Si−O network, the alkali ions would interact less strongly than if they were free. Nevertheless, the trends are expected to be similar to those computed for the free cations.

Ground-state singlet geometries (S_0) of ACP, MACP, and corresponding metal ion-coordinated systems were fully optimized at the B3LYP/6-31G* level. All stationary points were characterized as true minima on the potential energy surface by corresponding Hessian indices. All of the calculations were carried out using the Gaussian 98 series of programs.[24] Interaction energies were evaluated using the "super system" approach without the inclusion of basis set superposition error corrections. As illustrated in Figure 10, two binding modes (metal ion binding to the carbonyl oxygen, mode I, and to the phenyl ring, mode II) were identified in the case of ACP and three (in addition to modes I and II, binding to methoxy oxygen, mode III) in the case of MACP. All these geometries were used to compute the orbital energies and vertical excitation energies of

the triplet states. B3LYP/6-31G* calculations on adiabatic excited states in the triplet manifold yielded only the lowest-energy triplet state. Time-dependent density functional theory (TDDFT) calculations were performed to obtain a reliable estimate of the valence excitation energies.[25] Becke's three-parameter exchange[26] with LYP correlation functional[27] were used in conjunction with the 6-31+G* basis set. The TDDFT method uses Kohn−Sham density functional theory for the ground state and hence incorporates the dynamical electron correlation within the single-determinant formalism.[28] The quantitative accuracy of the TDDFT results tends to increase with cases where the valence excited states have substantial double-excitation character.[29] Another advantage of TDDFT from a qualitative point of view is the use of Kohn−Sham orbitals as the basis, which can provide a better understanding of various electronic transitions in a fairly straightforward fashion. In addition to the TDDFT, we have employed the single-reference configuration interaction method with all single excitations (CIS). In accordance with the standard recommendations for excited-state calculations, a basis set having diffuse as well as polarization functions was used (6-31+G* basis set) for both the TDDFT and CIS methods.[14b,30]

Computed binding affinities at the B3LYP/6-31G* level between Li^+ and Na^+ complexes with ACP and MACP are provided in Table 1. In binding mode I (Figure 10), the cation is bound to the carbonyl oxygen in near-collinear geometry. The interaction seems to be primarily electrostatic in nature when metal ions bind along the C=O bond dipole. Selected geometrical parameters are included in Table 1. It is clear that the C−O..M^+ angle is much closer to 180° than to 120°. For example, in the case of Li^+, the angle is 167°, and the cation is a few degrees (6°) above the CH_3C=O plane. Similar values are obtained in the case of Na^+ (168° and 0°). The same geometrical preference has been noted in all previous computational studies on alkali metal complexes of carbonyl compounds.[31] A Cambridge structural database analysis of metal ion binding to peptides has revealed that the metal ions tend to be located in the peptide plane along the C=O direction and not along the direction of the lone pair.[32a] The average M^+..O=C angle is identified to be in the range 140−170°. It may be of interest to note that the same type of analysis reveals that hydrogen bonding (X−H..O=C) occurs along the carbonyl lone pair.[32b,c] In the second mode of binding, the interaction is with the π electrons of the phenyl ring (cation−π interaction).[12] The lithium ion binding affinity with the carbonyl group is predicted to be 17.6 kcal/mol higher than with the phenyl group in ACP. The sodium ion was found to have only a quasilinear coordination with ACP through the carbonyl group. Attempts using Na^+..ACP with the initial geometry of the metal ion over the phenyl group resulted in the migration of the metal ion to the carbonyl group during geometry optimization. In the case of MACP, similar to ACP, interaction with the carbonyl oxygen is much stronger than with either the phenyl or methoxy groups. The difference between carbonyl versus phenyl binding affinities for MACP is 19.6 kcal/mol. It is interesting that the binding affinities of the lithium ion with the phenyl ring as well as with the methoxy groups are almost the same for MACP. Although no experimental data have been reported for ACP and MACP, the experimental binding affinities of alkali ions to carbonyl compounds such as acetaldehyde and acetone reported in the literature are in a range that is similar to that of the computed values in the present study.[33] We are aware that the B3LYP method slightly overestimates the ion−molecule binding energy.[33c] Since we are interested in the trends and range of binding

Alkali Ion-Controlled Ordering of Acetophenones

J. Phys. Chem. A, Vol. 107, No. 18, 2003 **3193**

TABLE 1: Computed Binding Affinities (kcal/mol) of Metal Ions with Acetophenone and 4′-Methoxyacetophenone

system	binding mode[a]	binding affinity kcal/mol		distance X^b..M^+ (Å)		angle X^b..M^+ (deg)		dihedral angle $CH_3C=O$..M^+ (deg)	
		S_0	T_1	S_0	T_1	S_0	T_1	S_0	T_1
Li^+..ACP	I	55.3	57.3	1.74	1.72	167.4	167.6	5.7	1.6
Li^+..ACP	II	37.7	47.2	1.89	1.85				
Na^+..ACP	I	39.9	39.8	2.10	2.08	168.6	162.0	0.1	0.1
Na^+..ACP	II		32.1		2.34				
Li^+..MACP	I	60.1	69.9	1.72	1.70	167.9	163.3	0.1	0.1
Li^+..MACP	II	40.5	47.7	1.89	1.85				
Li^+..MACP	III	39.0	47.6	1.86	1.80				
Na^+..MACP	I	43.7	51.1	2.08	2.06	169.1	162.5	0.2	0.1
Na^+..MACP	II		32.6		2.34				
Na^+..MACP	III	26.1	33.0	2.26	2.18				
Li^+..acetone	I	51.1	37.9	1.76	1.82	179.4	153.2	−29.1	113.4
Na^+..acetone	I	37.3	26.9	2.11	2.19	179.6	153.5	−32.3	112.5

[a] Mode I refers to the quasilinear binding of M^+ to the carbonyl oxygen. Mode II is the cation π-type binding, with M^+ over the phenyl ring. Binding of M^+ to the methoxy oxygen in MACP is referred as mode III. See Figure 10. [b] X represents the distance between the metal ion to the carbonyl oxygen in mode I, to the center of the phenyl ring in mode II, and to methoxy oxygen in mode III.

TABLE 2: Orbital Energies (eV) in the Singlet Ground State of Acetophenone and Its Derivative along with Corresponding Metal Ion-Coordinated Systems

system	binding mode	energies (eV) and the nature of the orbital				
ACP		−0.23, π_2*	−1.47, π_1*	−6.72, n	−7.01, π_2	−7.10, π_1
Li^+..ACP	I	−3.60, π_2*	−5.97, π_1*	−10.47, π_2	−10.70, π_1	−11.86, n
Li^+..ACP	II	−5.58, π_2*	−6.24, π_1*	−10.90, n	−12.36, π_1	−12.57, π_2
Na^+..ACP	I	−3.31, π_2*	−5.44, π_1*	−10.17, π_2	−10.34, π_1	−11.22, n
MACP		−0.20, π_2*	−1.19, π_1*	−6.22, π_1	−6.54, n	−7.06, π_2
Li^+..MACP	I	−3.47, π_2*	−5.53, π_1*	−9.62, π_1	−10.45, π_2	−11.49, n
Li^+..MACP	II	−5.35, π_2*	−5.72, π_1*	−10.63, n	−11.09, π_1	−12.35, π_2
Li^+..MACP	III	−4.58, π_2*	−4.95, π_1*	−9.84, n	−10.68, π_1	−11.28, π_2
Na^+..MACP	I	−3.19, π_2*	−5.03, π_1*	−9.27, π_1	−10.13, π_2	−10.88, n
Na^+..MACP	III	−4.20, π_2*	−4.71, π_1*	−9.68, n	−10.29, π_1	−10.95, π_2

affinity, we consider that the method is appropriate for the present purpose.

To explore the consequences of alkali metal ion binding on the nature of the excited states of ACP and MACP, we have employed several approaches. Since of the three modes of binding discussed above mode I is the most important and is more general (occurs with both Li^+ and Na^+), we discuss it first. According to B3LYP/6-31G* calculations, Li^+ and Na^+ ion binding to the carbonyl oxygen (mode I, Figure 10) results in the stabilization of the n orbital. Whereas the nature of the MOs is not altered in any significant manner, all of the MOs are shifted to lower energies through metal ion coordination. The key MOs of importance in the present context are the p-type n orbital on the carbonyl oxygen, the filled π_1 and π_2 orbitals, and the vacant π* orbitals. The n orbital is stabilized by Li^+ and Na^+ complexation to a greater extent than the π MOs, suggesting that the nπ* triplet will be shifted to higher energy because of cation binding (Table 2). On the basis of orbital energies, it is clear that unperturbed ACP will have nπ* and that ion-complexed ACP will have $\pi\pi$* as the lowest triplet. A similar analysis of MACP orbitals reveals that both unperturbed and ion-complexed MACP will have $\pi\pi$* as the lowest triplet. It is gratifying that we were able to predict the nature of the lowest triplet of unperturbed ACP and MACP correctly on the basis of orbital energies. Also, the prediction that the ion-bound ACP and MACP would have $\pi\pi$* as the lowest triplet is consistent with the photophysical studies presented in a previous section. The orbital energies of ACP and MACP bound to Li^+ and Na^+ in various modes are listed in Table 2. On the basis of orbital energies, one would predict that the triplet of MACP would be switched to nπ* when an alkali ion binds to it in modes II and III and that mode II binding to ACP would have no effect on the character of the lowest triplet (nπ*).

TABLE 3: Computed Excitation Energies (kcal/mol) of Acetophenone and Its Substituted Derivatives along with Corresponding Metal Ion-Coordinated Systems

system	binding mode[a]	B3LYP		TD-DFT		CIS	
		vertical	adiabatic	$\pi-\pi$*	n−π*	$\pi-\pi$*	n−π*
ACP		77.6	69.1 (74.2)[b]	77.2	74.5	72.8	98.5
Li^+..ACP	I	76.3	67.1	68.2	91.8	70.8	121.5
Li^+..ACP	II	70.6	59.6	86.0	66.4	79.8	93.1
Na^+..ACP	I	77.2	69.3	70.6	88.3	71.5	116.5
MACP		81.0	70.8 (71.4)[b]	73.6	76.8	74.9	101.2
Li^+..MACP	I	64.2	61.0	60.0	95.2	73.1	127.0
Li^+..MACP	II	74.0	63.6	80.5	70.6	81.6	96.1
Li^+..MACP	III	73.2	62.2	78.9	69.4	74.9	109.7
Na^+..MACP	I	67.7	63.5	63.0	91.1	74.0	121.0
Na^+..MACP	III	74.2	63.7	77.9	70.6	74.9	96.8

[a] Mode I refers to the quasilinear binding of M^+ to the carbonyl oxygen. Mode II is the cation π-type binding, with M^+ over the phenyl ring. Binding of M^+ to the methoxy oxygen in MACP is referred as mode III. See Figure 10. [b] Experimental value for $T_1 \rightarrow S_0$.

However, orbital energies are not always a reliable guide for deriving excited-state energetics. Adiabatic excited-state energies of the first triplet of free and ion-bound ACP and MACP were calculated at the B3LYP/6-31G* level (Table 3). On the basis of Kohn−Sham singly occupied orbitals, the lowest triplet of unperturbed ACP was characterized to be nπ* and calculated to be 69.1 kcal/mol above the ground state. The estimated triplet energy is slightly lower than the experimental value (74.2 kcal/mol). Characterization of the lowest triplet as nπ* is consistent with the experimental results in solution. Li^+ and Na^+ ion binding to ACP in mode I leads to a $\pi\pi$* triplet, whereas when Li^+ binds in mode II, the lowest triplet remains nπ*. State switching observed experimentally is consistent with the computational results. However, this method predicted the lowest triplet of MACP to be nπ* whereas it is known experimentally to be $\pi\pi$*. The estimated triplet energy is within
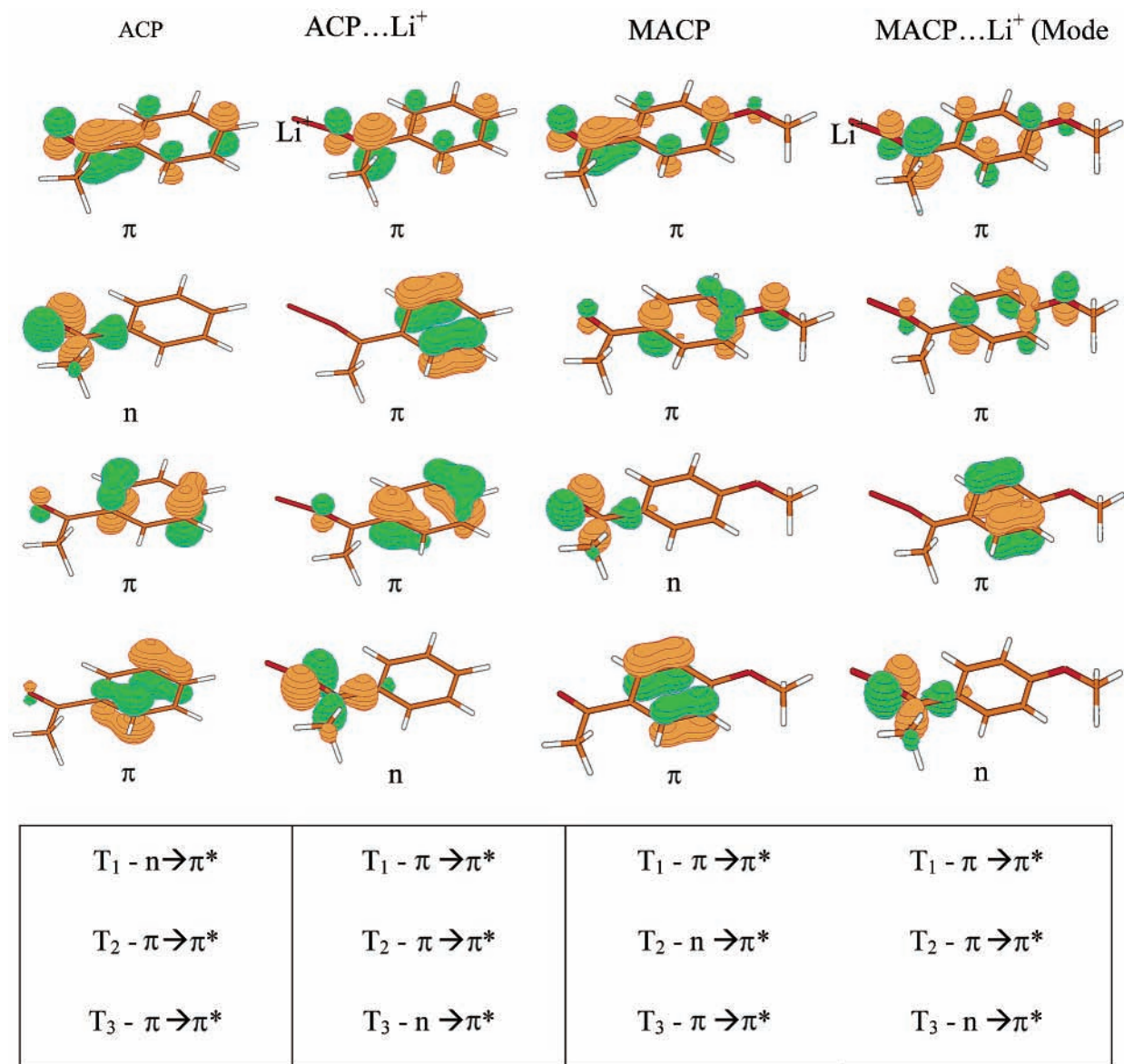
Figure 11. Relevant orbitals involved in the T_1, T_2, and T_3 transitions in the case of ACP and Li$^+$..ACP, MACP, and Li$^+$..MACP. Orbitals are generated along with the TDDFT/B3LYP/6-31+G*//B3LYP/6-31G* calculation. The nature of the excited states in a TDDFT calculation is assigned on the basis of the orbital contours for the initial and final orbitals involved in corresponding transitions.

a few kcal/mole from the experimental value. The fact that the B3LYP/6-31G* method failed to predict the lowest triplet of MACP correctly and also could not identify higher triplets led us to explore other options.

To estimate the vertical excitation energies, configuration interaction calculations were carried out at the CIS/6-31+G* level. Results obtained for unperturbed and ion-bound ACP and MACP are provided in Table 3. One disappointing fact was that the method did not correctly reproduce the nature of the lowest triplet of unperturbed ACP. Whereas it is known experimentally that ACP has nπ* as the lowest triplet, the computation suggested it to be $\pi\pi$* in nature. Problems of the same type have been noticed with the CIS method.[34] These are primarily due to the absence of dynamical correlation effects. Improvement in the CIS data can be achieved by the inclusion of double excitations using a perturbative scheme.[35,16c] Unfortunately, we have come across certain technical limitations due to the larger size and lower symmetry of systems considered in this study. Although the CIS method fails to give the correct ordering of states for ACP, it correctly predicted the nature of the lowest triplet of MACP.

A recent report that TDDFT gave the best prediction concerning electronic transition energies for alkyl ketones and aldehydes prompted us to employ this method in our studies.[16b] The vertical excitation energies computed at the TDDFT/6-31+G* level are listed in Table 3. The nature of the excited states in a TDDFT calculation are assigned on the basis of the orbital contours of the initial and final orbitals involved in corresponding transitions. Figure 11 lists the relevant Kohn–Sham orbitals for free and cation-bound ACP and MACP. Several results with respect to unperturbed ACP and MACP are noteworthy: (a) This method correctly predicts the nature of the lowest excited states of ACP (nπ*) and MACP ($\pi\pi$*). (b) The computed excitation energies of the lowest triplets for ACP and MACP are a few kcal/mol within the experimental (0,0) triplet energy values (ACP: computed, 74.5 kcal/mol; exptl, 74.2 kcal/mol; MACP: computed, 73.6 kcal/mol; exptl, 71.4 kcal/mol). (c) Consistent with the experimental results, the two lowest triplets (nπ* and $\pi\pi$*) are predicted to be in close in energy (<3.0 kcal/mol). Remarkable consistency between computed results and experimental observations gave us confidence in this method. The most significant computational result

Alkali Ion-Controlled Ordering of Acetophenones

J. Phys. Chem. A, Vol. 107, No. 18, 2003 **3195**

with respect to the zeolite is that within zeolites cation binding in mode I geometry would be the most favored (compare the binding affinities in Table 1) and when Li^+ and Na^+ bind to ACP and MACP in mode I the lowest triplet would be $\pi\pi^*$ in character (Table 3).

Whereas the computed TDDFT data refer to the vertical excitation energies within the Born–Oppenheimer approximation, we believe that the geometric relaxation will retain the predicted ordering of excited states. A more elaborate study necessitates the use of relaxed excited-state geometries, particularly when comparisons with emission studies are attempted. Effort was expended on finding the adiabatic excited states in connection with the present study. Despite exhaustive searches (at the B3LYP/6-31G* level), the second excited triplet states remained elusive. Several carefully chosen starting geometries with correct orbital sequences invariably ended up with the lowest excited states instead of the desired state. Close proximity combined with possibly large amount of mixing between $n\pi^*$ and $\pi\pi^*$ states for ACP and MACP might have prevented the proper convergence of the wave function to the desired state. The use of the complete active space self-consistent field (CASSCF) approach or complete active space second-order pertubation theory (CASPT2) might give a better idea of relaxed higher excited states.

Discussion

At 77 K, acetophenone in nonpolar as well as moderately polar organic solvents shows a structured emission (phosphorescence) with a short lifetime (millisecond range) characteristics of $n\pi^*$ states.[36] At 77 K, 4′-methoxyacetophenone shows a broad emission with a long lifetime (seconds) characteristics of $\pi\pi^*$ triplet state.[36] We have used these fingerprint features to identify the nature of the lowest triplet of acetophenones included within alkali ion-exchanged Y zeolites. As illustrated in Figure 2, two acetophenones within NaY show broad phosphorescence, suggesting that the emitting state is $\pi\pi^*$ in character. Further confirmation that the emitting state within NaY has $\pi\pi^*$ character comes from triplet lifetime measurements. As seen in Figure 4, the emitting state in the case of ACP–NaY has only one long component with a lifetime of 420 ms. It is important that the alkali ions that can interact strongly (Li^+, Na^+, and K^+) with the carbonyl chromophore show only $\pi\pi^*$-like phosphorescence. As opposed to ACP included in NaLiY, NaY, and NaKY, ACP included in NaRbY and NaCsY shows two emissions and two components for triplet decay that are characteristics of both $n\pi^*$ and $\pi\pi^*$ states. The fact that two lifetimes (Figure 4) and two emissions with different features are observed at different time slices (Figure 3) suggests that in these zeolites at 77 K ACP has two nonequilibrating closer-lying triplets. Triplet $n\pi^*$–$\pi\pi^*$ switching is a well-established phenomenon in ACP and related aryl alkyl ketones.[4,5] It has been established that in these ketones the nature of the lowest triplet depends on the polarity of the medium, the substituents on the ring, the ring size in the case of cyclic ketones (cyclophane-type structures), and the hydrogen-bonding ability of the medium.[4,36,37] The zeolite interior is known to be polar[19a] and may have the ability to form hydrogen bonds with ACP. However, the fact that these features are not responsible for the observed state switch within NaY comes from the observation that the co-inclusion of methanol, a polar molecule capable of hydrogen bonding, changes the nature of the lowest state from $\pi\pi^*$ to $n\pi^*$(Figure 5). If the polarity and hydrogen-bonding abilities of zeolites were responsible, then upon the inclusion of methanol, the $\pi\pi^*$ state should have been stabilized

instead of being destabilized. The fact that the nature of the emission and lifetime depends on the cation (Na^+ vs Cs^+) suggests that the triplet-state switching is likely to be controlled by the cation. More evidence in favor of this model comes from computational and solid-state NMR studies.

Density functional calculations (B3LYP/6-31G*) suggest that the Li^+ ion binds to ACP via two modes—dipolar interaction with carbonyl and cation–π interaction with the phenyl group (Figure 10). The binding affinities in the ground state are large, 55.3 and 37.7 kcal/mol, respectively (Table 1). Even in the triplet state the cation binding to ACP in these two modes is strong—binding affinities are 57.3 and 47.2 kcal/mol, respectively. In the case of the Na^+ ion, we could find only one minimum for ACP–Na^+ in its ground state (mode I), whereas in the triplet state, there were two minima (modes I and II). Of the two modes, binding to carbonyl is more stable than binding to the phenyl ring (39.8 vs 32.1 kcal/mol). On the basis of the above calculations, one would predict that within zeolites M^+ ion binding to ACP via carbonyl is more likely and ACP molecules would remain bound to the M^+ ion in the triplet state. As seen in Table 1, there are only slight differences in the geometries between the adiabatic triplet and the ground state of the ACP..Li^+ complex.

Note that the binding affinity as expected depends on the cation—Li^+ binds more strongly (55.3 kcal/mol) than Na^+ (39.9 kcal/mol). Although we have not performed calculations with K^+, Rb^+, and Cs^+, on the basis of the results with Li^+ and Na^+ (Table 1), we believe that binding affinity follows the trend $Li^+ > Na^+ > K^+ > Rb^+ > Cs^+$. Solid-state NMR results support this suggestion. Three independent measurements, static, MAS, and CP-MAS spectra of ^{13}C-enriched ACP included in MY zeolites, suggest that there is an interaction between the cation and ACP molecules: (a) The line width in the case of static and MAS spectra and signal intensity in the case of CP-MAS spectra depend on the cation (MY), suggesting that ACP molecules are less mobile in NaLiY and have more freedom in NaCsY. (b) The fact that ACP molecules are more mobile on silica, which has no cation, than within zeolites, which has at least four Type II cations in a supercage, brings out the importance of the cation···ACP interaction. (c) When NMR spectra of ACP in NaY zeolites of varying Si/Al ratios are compared, it is obvious that ACP molecules are more restricted within NaY of high alumina content (consequently, more cations). For example, ACP molecules are more restricted in Y zeolites with Si/Al 2.4 than in Y zeolites with Si/Al 40. (d) ACP molecules are mobile within hydrated rather than in dry NaY. These observations are consistent with the conclusion that within Y zeolites there is an interaction between ACP molecules and cations. Although NMR results do not provide information on the nature of the interaction, computational results suggest that the interaction between ACP and cations is likely to be dipolar in character.

The final aspect of the discussion deals with the consequence of cation binding on the ordering of excited triplet states. Of the various computational methods used, TDDFT alone was capable of correctly identifying several excited triplet states. This method correctly predicted the ordering in the case of cation-free ACP and MACP. Furthermore, the triplet energies calculated were a few kcal/mole (<2 kcal/mole) within experimental values. Even more impressive was the fact that the computed energy gaps between the $n\pi^*$ and $\pi\pi^*$ states in ACP and MACP were, which is consistent with the experimental observations (<5 kcal/mol). Consistency between the computed and experimental results with ACP and MACP gave us

3196 *J. Phys. Chem. A, Vol. 107, No. 18, 2003*

Shailaja et al.

confidence in the results obtained in the case of cation-bound ACP. As per TDDFT calculations, when Li$^+$ and Na$^+$ bind to ACP through the carbonyl oxygen, the $\pi\pi^*$ triplet is lower in energy than the nπ^* state (Table 3). As opposed to this, when Li$^+$ binds to ACP via the phenyl ring, the lowest triplet is predicted to have nπ^* character. The fact that the observed phosphorescence emission within NaLiY and NaY is characteristic of the $\pi\pi^*$ state suggests that the cations are bound to ACP via the carbonyl oxygen. This conclusion is also consistent with the binding affinities listed in Table 1; binding to carbonyl oxygen is energetically preferred. Further confirmation is provided by the photobehavior of MACP within zeolites. This molecule normally has a $\pi\pi^*$ state as the lowest triplet. According to the calculations, Li$^+$ could bind to MACP in three different modes (Figure 10). In two of these modes, binding to phenyl and to methoxy oxygen, MACP would have an nπ^* state as the lowest triplet. However, if the cation is bound to the carbonyl oxygen, the lowest triplet would remain $\pi\pi^*$ in character. Within zeolites as well as in solution, MACP has a $\pi\pi^*$ state as the lowest triplet (Figures 3 and 4). This suggests that the preferred binding with the cation is via the carbonyl oxygen. This observation is consistent with the conclusions drawn in the case of ACP. Also, on the basis of binding affinities, this would be expected (Table 1). Thus, when results of computation, solid-state NMR, and photophysical studies are viewed together, it is clear that triplet-state switching observed with ACP in MY zeolites is due to a cation···ACP interaction via the carbonyl oxygen.

A minor point we wish to draw attention relates to the variation in binding affinities between ACP and alkali ions in ground, nπ^* triplet, and $\pi\pi^*$ triplet states. As discussed above, the binding affinities in the case of ACP and MACP are similar in the ground and the excited triplet states ($\pi\pi^*$). However, acetone..M$^+$ with an nπ^* as the lowest triplet has lower binding affinities toward Li$^+$ and Na$^+$ than in the ground state (Table 1). This is expected on the basis of changes in the dipole moment between the ground state and the excited triplet state.[36] Because of the shift in electron density from the oxygen to the carbon, the nπ^* state is expected to have a lower dipole moment than the ground state. Since the interaction with alkali ions is driven by dipolar forces, a reduction in the dipole moment in the excited state would reduce the binding affinity, and it is nice that the calculations reproduce this result. The dipole moments for the $\pi\pi^*$ triplet and ground states are expected to be nearly the same; therefore, one would expect them to show similar affinity toward alkali ions. Computational data are also consistent with this expectation.

Conclusion

In this investigation, the phenomenon of triplet-state switching in aryl alkyl ketones within zeolites has been identified by changes in photophysical properties of acetophenones included within MY zeolites. Solid-state NMR measurements unequivocally suggest the existence of an interaction between alkali ions and acetophenone included within zeolites. A model based on computational data adequately accounts for the observed triplet-state switching within zeolites. The basic features of the model are the following: (a) Alkali ions present in zeolites interact with the carbonyl oxygen of the aryl alkyl ketone via a dipolar interaction. (b) In the triplet manifold, the alkali ion-bound aryl alkyl ketones, independent of the substituents on the phenyl ring, have a $\pi\pi^*$ state as the lowest triplet. An extension of this study leads us to predict that it should be possible to bring about a state switch in aryl alkyl and related ketones with close-lying

nπ^*−$\pi\pi^*$ triplet states via the use of an alkali ion salt. The realization of this possibility depends on our ability to dissolve alkali ion salts in organic solvents in such a way that the cations remain free to interact with solute molecules.

Experimental Section

Materials. Zeolites NaY (Si/Al 2.4) and HY (Si/Al 6, 15 and 40) were obtained from the PQ Corporation. Zeolites NaLiY, NaKY, and NaRbY were prepared from the NaY zeolite sample by conventional cation exchange using appropriate nitrate solution and refluxing at 90 °C for at least 3 h. A 10-mL aliquot of a 10% nitrate solution was used for each gram of zeolite, and the cation exchange was repeated three times. NaY zeolite samples (Si/Al 6, 15 and 40) were prepared from the HY zeolite using 10% sodium chloride solution. The exchanged samples were then thoroughly washed with water to remove sulfate and chloride ions. Exchange loading was typically between 60 and 84%. Commercial samples (Aldrich) of acetophenones were distilled twice prior to use.

Activation of Zeolite. About 300 mg of the zeolite was placed in a silica crucible and heated at 500 °C for 12 h. The freshly activated zeolite samples were rapidly cooled in air to ca. 50 °C and then transferred into glass sample tubes, connected to a vacuum manifold, and degassed at 80 °C under low pressure ($\sim$10^{-3} Torr). We observed that such a procedure not only facilitates the complete removal of water and other adsorbents but also makes it easier to transfer the evacuated sample into a glovebag.

Sample Preparation for Emission. The acetophenones were loaded into various cation-exchanged Y zeolites (activated at 500 °C in an oven) as a hexane slurry. The loading level was kept at 1 in 10 supercages. The samples were then washed with hexane and evacuated under vacuum (10^{-5} Torr) for at least 12 h. The evacuated samples were then cooled to 77 K using liquid nitrogen to carry out the photophysical studies.

Sample Preparation for Solid-State NMR. Acetophenone (99% enriched ^{13}C) was obtained from Cambridge Isotope Laboratories, Inc. About 4 mg of acetophenone (equivalent to 1 molecule per 4 supercages of MY zeolite) was added to 300 mg of activated zeolite in a glovebag under a nitrogen atmosphere. The sample was then mixed properly and degassed at 60 °C for typically 12 h under low pressure ($\sim$10^{-3} Torr). Such heating of the sample also ensures the uniform adsorption of acetophenone. In a glovebag under a nitrogen atmosphere, the degassed sample was then packed into a zirconia rotor having an O ring. ^{1}H NMR studies of these samples revealed that there was no adsorption of atmospheric moisture during the course of various NMR experiments.

Spectral Measurements. Absorption (Diffuse-Reflectance Mode). Absorption spectra were recorded on a Shimadzu 2101PC UV−vis spectrophotometer equipped with a diffuse reflectance accessory. The dried zeolite samples were packed into a 2-mm quartz cuvette (in a drybox) and sealed with Teflon tape. The reflectance spectra were converted to absorption by using a Kubelka−Munk program supplied with the instrument. The solution spectra were recorded in 10-mm quartz cells using solvent as the reference.

Steady-State Emission. Emission spectra were recorded on an Edinburgh FS-900 CDT spectroflourimeter with a 500-W xenon lamp as the light source. Solid zeolite samples were loaded into quartz electron-spin resonance (ESR) tubes placed in a quartz cylindrical dewar, and the emission collected at right angles was recorded. Phosphorescence spectra were recorded at 77 K using liquid nitrogen as the coolant.

Alkali Ion-Controlled Ordering of Acetophenones

J. Phys. Chem. A, Vol. 107, No. 18, 2003 **3197**

Time-Resolved Emission. Time-resolved phosphorescence measurements were performed by multichannel scaling on an OB900 fluorometer (Edinburgh Analytical Instruments) using a pulsed xenon lamp as the excitation source (μF, Edinburgh Analytical Instruments) with a pulse length of approximately 10 μs. Solid samples were placed in quartz tubes (3-mm diameter) and were evacuated (ca. 5×10^{-5} Torr) to remove oxygen and water. All time-resolved spectral measurements were made at 77 K using a liquid-nitrogen dewar. The samples were excited at 320 nm. An average of 100 decay traces were recorded at each monitoring wavelength at a 5-nm interval. The spectra at individual time intervals were obtained by slicing the decay traces accordingly.

Solid-State NMR Spectra. Solid-state ^{13}C NMR were recorded at room temperature with a Bruker AVANCE DSX 300 spectrometer at a ^{13}C resonance frequency of 75.47 MHz. Each acquisition typically consisted of 12 000 to 16 000 free-induction decay scans. The ^{13}C Bloch decay (^{13}C BD) spectra with high-power ^{1}H decoupling were acquired without (static) and with magic-angle spinning (MAS, spinning rate 4 kHz). The 90° pulse width used was 6.5 μs, and a recycle delay of 4 s was used for all of the samples. The ^{1}H$-^{13}$C cross-polarization spectra (^{13}C CP-MAS) were obtained with a recycle delay of 2 s using a 90° pulse width of 6.5 μs and a contact time of 1.5 ms. All CP-MAS experiments were processed with line broadening at 100 Hz, whereas Bloch decay experiments were processed with 10-Hz line broadening. The spectra were referenced at room temperature relative to TMS. All NMR figures were plotted using Bruker XWINPlot software.

Computations. Ground-state singlet and lowest triplet excited-state geometries (S_0 and T_1) of acetophenone (ACP), 4′-methoxy acetophenone (MACP), and corresponding metal ion-coordinated systems were fully optimized at the B3LYP/6-31G* level. All stationary points were characterized as true minima on the potential energy surface by corresponding Hessian indices. All of the calculations were carried out using the Gaussian 98 series of programs. Time-dependent density functional theory (TD-DFT) calculations were performed to find the valence excitation energies. Becke three-parameter exchange with LYP correlation functionals were used in conjunction with the 6-31+G* basis set. We have employed the single-reference configuration interaction method with all single excitations (CIS). In accordance with the standard recommendations for excited-state calculations, a basis set having diffuse as well as polarization functions was used (6-31+G* basis set).

The nature of each electronic transition was assigned by a careful examination of the orbitals involved in the corresponding transitions. The orbital contours for the Kohn−Sham orbitals were generated using the Molden (version 3.6) program. Orbital contour plots were generated either with the Gaussview or Molden (version 3.6) programs.

References and Notes

(1) (a) Kasha, M. *Faraday Discuss. Chem. Soc.* **1950**, *9*, 14−19. (b) Kasha, M. *Radiat. Res.* **1960**, *Supplement 2*, 243−275.

(2) (a) Zimmerman, H. E. *Tetrahedron* **1963**, *19*, 393−401. (b) Dauben, W. G.; Salem, L.; Turro, N. J. *Acc. Chem. Res.* **1975**, *8*, 41−54.

(3) (a) Moore, W. M.; Hammond, G. S.; Foss, R. P. *J. Am. Chem. Soc.* **1961**, *83*, 2789−2794. (b) Hammond, G. S.; Baker, W. P.; Moore, W. M. *J. Am. Chem. Soc.* **1961**, *83*, 2795−2799.

(4) (a) Wagner, P. J. Triplet States III. In *Topics in Current Chemistry*; Springer-Verlag: Berlin, 1976; Vol. 66, pp 1−52. (b) Wagner, P. J.; Park, B. -S. In *Organic Photochemistry*; Padwa, A.; Ed.; Marcel Dekker: New York, 1991; Vol. 11, pp 227−366. (c) Favaro, G. *J. Photochem.* **1982**, *20*, 33−46.

(5) (a) Lamola, A. A. *J. Chem. Phys.* **1967**, *47*, 4810−4816. (b) Rauh, R. D.; Leermakers, P. A. *J. Am. Chem. Soc.* **1968**, *90*, 2246−2249.

(6) (a) Yang, N. C.; McClure, D. S.; Murov, S. L.; Houser, J. J.; Dusenbury, R. *J. Am. Chem. Soc.* **1967**, *89*, 5466−5468. (b) Yang, N. C.; Dusenbury, R. L. *J. Am. Chem. Soc.* **1968**, *90*, 5899−5900. (c) Wagner, P. J.; Siebert, E. J. *J. Am. Chem. Soc.* **1981**, *103*, 7329−7335. (d) Wagner, P. J.; Kemppainen, A. E.; Schott, H. N. *J. Am. Chem. Soc.* **1973**, *95*, 5604−5614. (e) Nakayama, T.; Sakurai, K.; Ushida, K.; Kawatsura, K.; Hamanoue, K. *Chem. Phys. Lett.* **1989**, *164*, 557−561. (f) Nakayama, T.; Sakurai, K.; Ushida, K.; Hamanoue, K.; Otani, A. *J. Chem. Soc., Faraday Trans.* **1991**, *87*, 449−454.

(7) (a) Uppili, S.; Ramamurthy, V. *Org. Lett.* **2002**, *4*, 87−90. (b) Uppili, S.; Takagi, S.; Sunoj, R. B.; Lakshminarasimhan, P.; Chandrasekhar, J.; Ramamurthy, V. *Tetrahedron Lett.* **2001**, *42*, 2079−2083. (c) Sunoj, R. B.; Lakshminarasimhan, P.; Ramamurthy, V.; Chandrasekhar, J. *J. Comput. Chem.* **2001**, *22*, 1598−1604.

(8) (a) Fukuzumi, S.; Itoh, S. *Adv. Photochem.* **1999**, *25*, 107. (b) Fukuzumi, S. *Bull. Chem. Soc. Jpn.* **1997**, *70*, 1. (c) Fukuzumi, S.; Fujii, Y.; Suenobu, T. *J. Am. Chem. Soc.* **2001**, *23*, 1019. (d) Fukuzumi, S.; Mori, H.; Imahori, H.; Suenobu, T.; Araki, Y.; Ito, O.; Kadish, K. M. *J. Am. Chem. Soc.* **2001**, *123*, 12458. (e) Fukuzumi, S.; Satoh, N.; Okamoto, T.; Yasui, K.; Suenobu, T.; Seko, Y.; Fujitsuka, M.; Ito, O. *J. Am. Chem. Soc.* **2001**, *123*, 7756. (f) Itoh, S.; Kumei, H.; Nagatomo, S.; Kitagawa, T.; Fukuzumi, S. *J. Am. Chem. Soc.* **2001**, *123*, 2165.

(9) (a) Van-Bekkum, H.; Flanigen, E. M.; Jansen, J. C. *Introduction to Zeolite Science and Practice;* Elsevier: Amsterdam, 1991. (b) Dyer, A. *An Introduction to Zeolite Molecular Sieves;* Wiley & Sons: New York, 1988. (c) Breck, D. W. *Zeolite Molecular Sieves: Structure, Chemistry and Use;* Wiley & Sons: New York, 1974.

(10) (a) Shepelev, Y. F.; Butikova, I. K.; Smolin, Y. I. *Zeolites* **1991**, *11*, 287. (b) Shepelev, Y. F.; Andersen, A. A.; Smolin, Y. I. *Zeolites* **1990**, *10*, 61. (c) Takaishi, T. *Zeolites* **1996**, *17*, 389. (d) Olson, D. H. *Zeolites* **1995**, *15*, 439. (e) Forano, C.; Slade, R. C. T.; Andersen, E. K.; Andersen, I. G. K.; Prince, E. *J. Solid State Chem.* **1989**, *82*, 95. (f) Malek, A.; Ozin, G. A.; Macdonald, P. M. *J. Phys. Chem.* **1996**, *100*, 16662. (g) Yeom, Y. H.; Jang, S. B.; Kim, Y.; Song, S. H.; Seff, K. *J. Phys. Chem. B* **1997**, *101*, 6914.

(11) (a) Mellot, C.; Simonot-Grange, M.-H.; Pilverdier, E.; Bellat, J.-P.; Espinat, D. *Langmuir* **1995**, *11*, 1726. (b) Fitch, A. N.; Jobic, H.; Renouprez, A. *J. Chem. Soc. Chem. Commun.* **1985**, 284. (c) Fitch, A. N.; Jobic, H.; Renouprez, A. *J. Phys. Chem.* **1986**, *90*, 1311. (d) Jobic, H.; Renouprez, A.; Fitch, A. N.; Lauter, H. J. *J. Chem. Soc., Faraday Trans.* **1987**, *83*, 3199. (e) Goyal, R.; Fitch, A. N.; Jobic, H. *J. Chem. Soc., Chem. Commun.* **1990**, 1152. (f) Klein, H.; Kirschhock, C.; Fuess, H. *J. Phys. Chem.* **1994**, *98*, 12345. (g) Czjzek, M.; Fuess, H.; Vogt, T. *J. Phys. Chem.* **1991**, *95*, 5255. (h) Pichon, C.; Methivier, A.; Grange, M.-H. S.; Baerlocher, C. *J. Phys. Chem. B* **1999**, *103*, 10197. (i) Vitale, G.; Mellot, C. F.; Bull, L. M.; Cheetham, A. K. *J. Phys. Chem. B* **1997**, *101*, 4559. (j) Yeom, Y. H.; Kim, A. N.; Kim, Y.; Song, S. H.; Seff, K. *J. Phys. Chem. B* **1998**, *102*, 6071. (k) Pichon, C.; Methivier, A.; Grange, M.-H. S.; Baerlocher, C. *J. Phys. Chem. B* **1999**, *103*, 10197.

(12) (a) Gokel, G. W.; De Wall, S. L.; Meadows, E. S. *Eur. J. Org. Chem.* **2000**, *17*, 2967. (b) Ma, J. C.; Dougherty, D. A. *Chem. Rev.* **1997**, *97*, 1303. (c) Kim, K. S.; Tarakeshwar, P.; Lee, J. Y. *Chem. Rev.* **2000**, *100*, 4145. (d) Fujii, T. *Mass Spectrom. Rev.* **2000**, *19*, 111.

(13) Kirschhock, C.; Fuess, H. *Zeolites* **1996**, *17*, 381.

(14) (a) Lim, K. H.; Grey, C. P. *J. Am. Chem. Soc.* **2000**, *122*, 9768. (b) Lim, K. H.; Jousse, F.; Auerbach, S. M.; Grey, C. P. *J. Phys. Chem. B* **2001**, *105*, 9918. (c) Jaramillo, E.; Grey, C. P.; Auerbach, S. M. *J. Phys. Chem. B* **2001**, *105*, 12319. (d) Grey, C. P.; Poshini, I. F.; Gualtieri, A. F.; Norby, P.; Hanson, J. C.; Corbin, D. R. *J. Am. Chem. Soc.* **1997**, *119*, 1981. (e) Norby, P.; Poshini, F. I.; Gualtieri, A. F.; Hanson, J. C.; Grey, C. P. *J. Phys. Chem. B* **1998**, *102*, 839.

(15) (a) Beagley, B.; Dwywr, J.; Fitch, F. R.; Zanjanchi, M. A. *J. Inclusion Phenom.* **1985**, *3*, 143−149. (b) Rubio, J. A.; Soria, J.; Cano, F. H. *J. Colloid Interface Sci.* **1980**, *73*, 312.

(16) (a) Hadad, C. M.; Foresman, J. B.; Wiberg, K. B. *J. Phys. Chem.* **1993**, *97*, 4293−4312. (b) Wiberg, K. B.; Stratmann, R. E.; Frisch, M. J. *Chem. Phys. Lett.* **1998**, *297*, 60−64.

(17) Li, Y. H.; Lim, E. C. *Chem. Phys. Lett.* **1970**, *7*, 15−18.

(18) (a) Kasha, M. *J. Chem. Phys.* **1952**, *20*, 71−74. (b) McClure, D. S. *J. Chem. Phys.* **1949**, *17*, 905−913. (c) Ramamurthy, V.; Caspar, J. V.; Eaton, D. F.; Kuo, E. W.; Corbin, D. R. *J. Am. Chem. Soc.* **1992**, *114*, 3882−3892.

(19) We earlier determined that micropolarity is responsible for the triplet-state switching of enones within zeolites: (a) Uppili, S.; Thomas, K. J.; Crompton, E. M.; Ramamurthy, V. *Langmuir* **2000**, *16*, 265−274. (b) Jayathirtha Rao, V.; Uppili, S.; Corbin, D. R.; Schwarz, S.; Lustig, S. R.; Ramamurthy, V. *J. Am. Chem. Soc.* **1998**, *120*, 2480.

(20) Cizmeciyan, D.; Sonnichsen, L. B.; Garcia-Garibay, M. A. *J. Am. Chem. Soc.* **1997**, *119*, 184.

(21) Barich, D. H.; Nicholas, J. B.; Xu, T.; Haw, J. *J. Am. Chem. Soc.* **1998**, *120*, 12342.

(22) (a) Schaefer, J.; Stejskal, E. O. *J. Am. Chem. Soc.* **1976**, *98*, 1031. (b) Schaefer, J.; Stejskal, E. O. *Top. Carbon-13 NMR Spectrosc.* **1979**, *3*, 283. (c) Stejskal, E. O.; Memory, J. D. *High-Resolution NMR in the Solid State;* Oxford University Press: New York, 1994.

(23) Ramamurthy, V. In *Photochemistry in Organized and Confined Media;* Ramamurthy, V., Ed.; VCH Publishers: New York, 1991; p 429.

(24) Frisch, M. J.; Trucks, G. W.; Schlegel, H. B.; Scuseria, G. E.; Robb, M. A.; Cheeseman, J. R.; Zakrzewski, V. G.; Montgomery, J. A., Jr.; Stratmann, R. E.; Burant, J. C.; Dapprich, S.; Millam, J. M.; Daniels, A. D.; Kudin, K. N.; Strain, M. C.; Farkas, O.; Tomasi, J.; Barone, V.; Cossi, M.; Cammi, R.; Mennucci, B.; Pomelli, C.; Adamo, C.; Clifford, S.; Ochterski, J.; Petersson, G. A.; Ayala, P. Y.; Cui, Q.; Morokuma, K.; Malick, D. K.; Rabuck, A. D.; Raghavachari, K.; Foresman, J. B.; Cioslowski, J.; Ortiz, J. V.; Stefanov, B. B.; Liu, G.; Liashenko, A.; Piskorz, P.; Komaromi, I.; Gomperts, R.; Martin, R. L.; Fox, D. J.; Keith, T.; Al-Laham, M. A.; Peng, C. Y.; Nanayakkara, A.; Gonzalez, C.; Challacombe, M.; Gill, P. M. W.; Johnson, B. G.; Chen, W.; Wong, M. W.; Andres, J. L.; Head-Gordon, M.; Replogle, E. S.; Pople, J. A. *Gaussian 98*, revision A.6; Gaussian, Inc.: Pittsburgh, PA, 1998.

(25) Casida, M. E.; Jamorski, C.; Casida, K. C.; Salahub, D. R. *J. Chem. Phys.* **1998**, *108*, 4439.

(26) Becke, A. D. *Phys. Rev. A* **1988**, *38*, 3098.

(27) Lee, C.; Yang, W.; Parr, R. G. *Phys. Rev. B* **1988**, *37*, 785.

(28) Casida, M. In *Recent Advances in Density Functional Methods;* Chong, D. P., Ed.; World Scientific Press: Singapore, 1995; Vol. I, p 155.

(29) (a) Bauernschmitt, R.; Ahlrichs, R. *Chem. Phys. Lett.* **1996**, *256*, 454. (b) Bauernschmitt, R.; Ahlrichs, R.; Hennrich, F. H.; Kappes, M. M. *J. Am. Chem. Soc.* **1998**, *120*, 5052.

(30) (a) Foresman, J. B.; Head-Gordon, M.; Pople, J. A.; Frisch, M. J. *J. Phys. Chem.* **1992**, *96*, 135. (b) Clark, T.; Chandrasekhar, J.; Spitznagel, G. W.; Schleyer, P. v. R. *J. Comput. Chem.* **1983**, *4*, 294.

(31) (a) Smith, S. F.; Chandrasekhar, J.; Jorgensen, W. L. *J. Phys. Chem.* **1982**, *86*, 3308. (b) Raber, D.; Raber, N. J.; Chandrasekhar, J.; Schleyer, P. v. R. *Inorg. Chem.* **1984**, *23*, 4076. (c) Ha, T.; Wild, U. P.; Kuhne, R. O.; Loesch, C.; Schaffhauser, T.; Stachel, J.; Wokaum, A. *Inorg. Chem.* **1978**, *61*, 1193. (d) Del Bene, J. E. *Chem. Phys.* **1979**, *40*, 329. (e) Del Bene, J. E.; Frisch, M. J.; Raghavachari, K.; Pople, J. A.; Schleyer, P. v. R. *J. Phys. Chem.* **1983**, *87*, 73. (f) Del Bene, J. E. *Chem. Phys. Lett.* **1979**, *64*, 227−229.

(32) (a) Chakrabarti, P. *Biochemistry* **1990**, *29*, 651−658. (b) Steiner, T.; Desiraju, G. R. *J. Chem. Soc., Chem. Commun.* **1998**, 891−892. (c) Steiner, T.; Kanters, J. A.; Kroon, J. *J. Chem. Soc., Chem. Commun.* **1996**, 1277−1278.

(33) (a) Staley, R. H.; Beauchamp, J. L. *J. Am. Chem. Soc.* **1975**, *97*, 5920−5921. (b) Guo, B. C.; Conklin, B. J.; Castleman, A. W. J. *J. Am. Chem. Soc.* **1989**, *111*, 6506−6510. (c) Armentrout, P. B.; Rodgers, M. T. *J. Phys. Chem. A* **2000**, *104*, 2238−2247. (d) McMahon, T. B.; Ohanessian, G. *Chem.−Eur. J.* **2000**, *6*, 2931−2941.

(34) (a) Maurice, D.; Head-Gordon, M. *J. Phys. Chem.* **1996**, *100*, 6131. (b) Hirata, S.; Head-Gordon, M. *Chem. Phys. Lett.* **1999**, *302*, 375. (c) Foresman, J. B.; Schlegel, H. B. In *Recent Experimental and Computational Advances in Molecular Spectroscopy;* Fausto, R., Ed.; Kluwer Academic Publishers: Norwell, MA, 1993; p 11.

(35) (a) Head-Gordon, M.; Rico, R. J.; Oumi, M.; Lee, T. J. *Chem. Phys. Lett.* **1994**, *219*, 21. (b) Head-Gordon, M.; Maurice, D.; Oumi, M. *Chem. Phys. Lett.* **1995**, *246*, 114.

(36) Turro, N. J. *Modern Molecular Photochemistry;* University Science Press: Mill Valley, CA, 1991.

(37) Turro, N. J.; Gould, I. R.; Liu, J.; Jenks, W. S.; Staab, H.; Alt, R. *J. Am. Chem. Soc.* **1989**, *111*, 6378−6383.